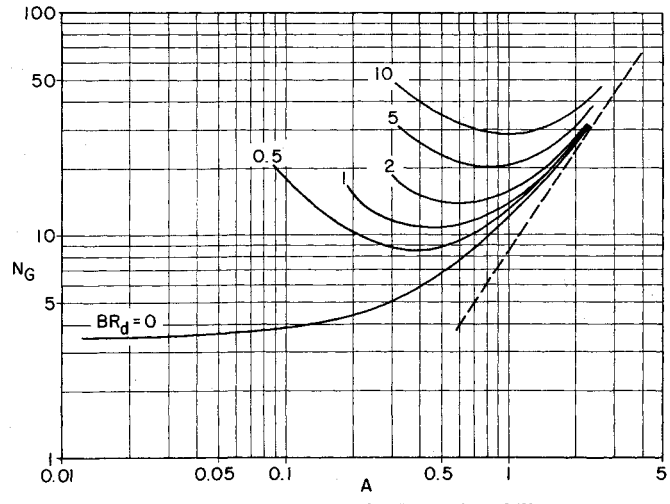

Fig. 3 Amplification curves for Type I instability.

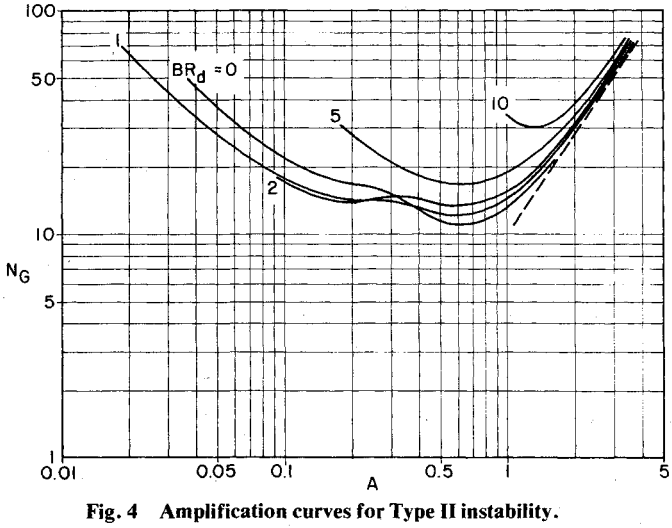

Fig. 4 Amplification curves for Type II instability.

Figures 3 and 4 are calculated spatial amplification curves for the Type I and Type II perturbations, respectively. By eliminating the characteristic length δ from the definition of the Görtler number and the dimensionless wavenumber ($=\alpha\delta = 2\pi\delta/s$, where λ is the lateral wavelength), one obtains $N_G^2/A^3 = U_s^2\lambda^3/8\lambda^2\nu^2 R_0$, where R_0 is the radius of curvature of the plate. If U_s, R_0, and λ remain constant with increasing x, then N_G^2/A^3 becomes a constant C_0. This is represented by the dashed line of gradient *3/2* on the log-log plots of Fig. 4. When the constant C_0 has a value at which the straight line is below the neutral curve, the vortices with the wavelength λ corresponding to C are damped spatially owing to viscous effects. When $C \geq 72.3$ for the Type I instability or ≥ 97.8 for the Type II instability, the straight line touches or cuts the neutral curve and the walljet enters an unstable region. These values of C are not too different from the corresponding value ($C \sim 78$) calculated for the laminar boundary layer and the asymptotic suction profile from the results of Smith[1] and Kobayashi,[4] respectively.

It is rather interesting that both the Type I and II amplification curves appear to be tangential to the line of *3/2* gradient. This indicates that vortex wavelength in this region is highly selective and spatial amplification would occur at constant wavelength until nonlinear effects became important.

Conclusion

An analysis of centrifugal instability in walljets along curved surfaces has been performed using linear perturbation theory. Instability on concave as well as convex walls has been investigated. For a given Reynolds number as well as radius of curvature, it is found that the walljet is more unstable on a concave wall than on a convex one. The work reported here could also find application in turbulent walljets. Tani[5] has demonstrated the utility of stability calculations of Taylor-Görtler vortices applied to turbulent boundary layers.

References

[1] Smith, A.M.O., "On the Growth of Taylor-Görtler Vortices along Highly Concave Walls," *Quarterly of Applied Mathematics*, Vol. 13, 1955, pp. 233-262.

[2] Glauert, M. B., "The Walljet," *Journal of Fluid Mechanics*, Vol. 1, 1956, pp. 625-643

[3] Conte, S. D., "The Numerical Solution of Linear Boundary Value Problems," *SIAM Review*, Vol. 8, No. 3, 1966, pp. 309-321.

[4] Kobayashi, R., "Note on the Stability of a Boundary Layer on a Concave Wall with Suction," *Journal of Fluid Mechanics*, Vol. 52, Pt. 2, 1972, pp. 269-272.

[5] Tani, I., "Production of Longitudinal Vortices in the Boundary Layer along a Concave Wall," *Journal of Geophysical Research*, Vol. 67, No. 8, 1962, pp. 3075-3080.

Gravitational Effects on Process-Induced Defects in Single Crystal Silicon

W.A. Porter* and D.L. Parker†
Texas A&M University, College Station, Tex.

FOR the past several years semiconductor manufacturers have been concerned with imperfections that are induced during device fabrication. Considerable effort has been directed toward understanding the causes of these dislocations.[1,2] Various processing steps have been identified as major contributors to the generation of dislocations. During diffusion, thermal gradients sufficient to cause the generation of dislocations are produced.[3] Impurity depositions lead to concentration gradients which produce stresses that result in dislocation creation.[4] It is also known that the thermal mismatch of the oxide at the oxide-silicon interface can lead to the generation of undesirable imperfections in the wafer.[5]

While these steps have been identified as crucial ones in controlling process-induced dislocations, the critical conditions present when the dislocations are generated during each step have not been determined. To understand the exact conditions present when dislocations are generated in any one of these steps requires that one be able to separate the various influencing factors. It is necessary, then, to be able to create the dislocations selectively while maintaining control of all the critical parameters. One critical parameter which has been largely ignored is the gravitational stress in the wafer, which is ever present in earth-bound processing experiments.

This parameter alone leads to important questions concerning possible advantages for space production of semiconductor devices. Previous emphasis has been on semiconductor crystal growth, although starting material quality produced on earth is considerably better than that which can be maintained during earth processing. This paper discusses a series of

Presented as Paper 74-647 at the AIAA/ASME 1974 Thermophysics and Heat Transfer Conference. Boston, Mass., July 15-17, 1974; submitted April 1,1975; revision recieved July 28, 1975. This project supported by NASA contract NAS8-29851.

Index categories: Materials, properties of; Atomic, Molecular, and Plasma Properties.

*Director Institute for Solid State Electronics.

†Assistant Professor, Department of Electrical Engineering.

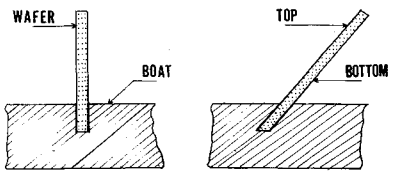

Fig. 1 Wafer orientation.

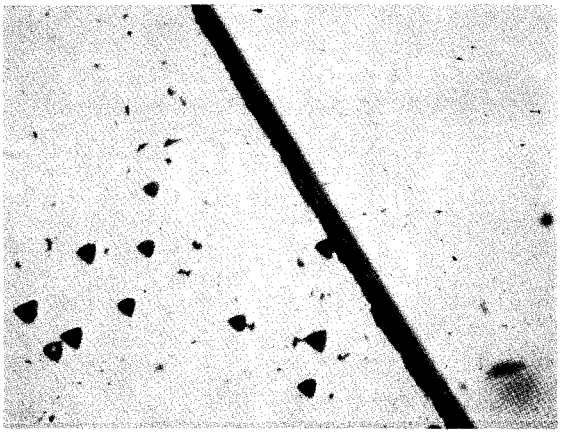

Fig. 2 Dislocation comparison with 175X Microscope.

experiments which vary each of several important processing parameters, including wafer orientation, temperature, gravity greater than 1 *g*, and ultimately zero gravity. These experiments are in progress and results to date are included from experiments which control 1) temperature, 2) duration of thermal cycle, and 3) wafer orientation during 1-*g* processing. Preliminary evidence is presented which indicates that gravitational stresses do play a role in defect generation during processing at 1 *g*.

Proposed Experiments

In view of the long time duration required for thermal processing of silicon, no practical low-gravity experiments are possible with drop towers or even rocket flights. However, this does not mean that useful information on the role played by gravity cannot be obtained without orbiting experiments. The following is a logical sequence of experiments which will allow maximum control of all the critical parameters for identification of the role played by each in producing lattice defects.

Open Tube Experiments

These experiments are done in conventional production type furnaces. Various means of supporting and orientating the wafer allows some control over the distribution of gravitational stress on the wafer in a 1-*g* environment. The purposes of these experiments are to demonstrate the gravitational effect, study *combinations* of the critical parameters, and to correlate and interpret results obtained with sealed ampule experiments. Some results obtained from these experiments are included later in this paper.

Sealed Ampule Experiments at 1-*g*

Considerations of safety, convenience, and control require the use of sealed ampules for initial satellite processing tests. Interpretation will require considerable familiarity with the results obtained from otherwise identical tests at 1-*g*. The sealed ampule processing technique will also prove convenient for multi-*g* experiments.

Multi-*g* Experiments

Once the sealed ampule processing technique is established a small furnace on a centrifuge will allow considerable enhancement of the gravitational effects and perhaps extrapolated predictions of what may be expected under zero-gravity conditions.

Zero-Gravity Experiments

Only extensive research in orbiting space laboratories will answer all the important technological and economic questions related to space manufacturing of semiconductor devices. However, a few relatively simple experiments should be sufficient to determine the role played by gravity on the well-known (but not well-understood) phenomenon of plastic flow.

Experimental Procedure and Results

The primary objective of these initial experiments was to demonstrate the influence of gravity on creating dislocations in silicon wafers during thermal cycling. Thus, thermal cycling of silicon wafers was performed in a controlled ambient where no impurities were present and oxidation was minimum. Both $n-$ and $p-$ type silicon wafers having a diameter of 1.25-1.5 in. with $\{111\}$ orientation and 8-16 Ω-cm resistivity were used. These wafers were positioned either individually or in pairs on a specially designed quartz carrier which supports the wafer at the bottom edge. The carrier has slots which allow the wafers to be supported either vertically or at a 45° cantilevered position. Figure 1 shows the wafer-carrier configuration.

Using the carrier described, wafers were first cycled vertically varying: 1) the insertion-withdrawal rate and 2) the time in the furnace. From these experiments an insertion-withdrawal rate of 2 in./min up to 1250°C was established as an optimum rate which prevents dislocation generation due to thermal gradients. The length of time the wafer is in the furnace influences lattice defects primarily through the plastic-flow phenomenon.

Using the 2 in./min insertion-withdrawal rate established during the vertical cycling experiments, wafers were cycled in the 45° cantilivered position in the following ways: 1) two wafers, one with the polished side up and one with the polished side down, 2) wafers with both sides polished. It is important to note in this case that the gravitational stress produces a compressional deformation on the bottom side of the wafer and a stretching deformation on its top side. These experiments were run with furnace temperatures ranging between 1000°C and 1250°C. After thermal cycling, each wafer was given a 2-min etch to remove the (very thin) oxide. Then, a sequence of Sirtl etches was performed with a total Sirtl etch time of 5 min. The dislocation density on the polished side was determined using the standard ASTM 9 position measurement technique under a 175X light microscope. Figure 2 shows the relative dislocation densities for wafers cycled at 45° with the polished side down shown in the left-lower portion of the picture and polished side up shown in the upper-right portion. Table 1 gives average dislocation densities for the five ASTM points nearest the center of the wafer

Table 1 Average dislocation density near center of wafers

Sample No.	Temperature, °C	Time, hr	Polished Side	Dislocation count	Average dislocation density (per cm^2)
82	1100	3	Both	Top	1860
82	1100	3	Both	Bottom	4410
83	1150	3	Up	Top	435
84	1150	3	Down	Bottom	1050

for three typical runs: one wafer polished and inspected on both sides (#82) and two wafers (#83 & #84) cycled simultaneously, one with the polished side up and the other with the polished side down.

The quantitative dislocation density fluctuates from run to run but, for a given run, the wafer with the polished side down *always* has more dislocations than the one with the polished side up. The difference in densities from run to run has not yet been explained, but the strong correlation between top and bottom dislocation densities for a given run is preliminary evidence that gravity influences the creation of lattice defects.

References

[1] Schwuttke, G. H., and Fairfield, J. M., "Dislocations in Silicon due to Localized Diffusion," *Journal of Applied Physics*, Vol. 37, No. 12, Nov. 1966, pp. 4394-4396.

[2] Plantinga, G.H., "Influence of Dislocations on Properties of Shallow Diffused Transistors," *IEEE Transactions on Electron Devices*, Vol. ED 16, No. 4, April 1969, pp. 394.

[3] Hu, S.M., "Temperature Distribution and Stress in Circular Wafers in a Row during Radiative Cooling," *Journal of Applied Physics*, Vol. 40, Oct. 1969, pp. 4413-4423.

[4] Parker, T.J., "Diffusion in Silicon. I. Effect of Dislocation Motion on the Diffusion Coefficients of Boron and Phosphorus in Silicon," *Journal of Applied Physics*, Vol. 38, Aug. 1967, pp. 3471-3474.

[5] Jaccodine, R. J. and Schlegel, W. A., "Measurement of Strains at Si-SiO_2 Interface," *Journal of Applied Physics*, Vol. 37, May 1966, pp. 2429-2434.

Solutions of Laplace's Equation in a Rectangle with a Large Hole

A. K. Naghdi*
Indiana University–Purdue University at Indianapolis, Indianapolis, Ind.

EMPLOYING a new technique, the even eigenfunctions of Laplace's equation in a rectangular region with a large central circular hole are derived. The eigenfunctions, satisfying homogeneous outer boundary conditions are generated by the integration on circular paths of the single series form of Green's function obtained with a method somewhat different from the classical techniques. The solutions so obtained are then linearly combined to meet the nonhomogeneous condition at the boundary of the circular hole. The technique is employed to the solutions of the problems of torsion of prismatic bars and steady-state two-dimensional heat conduction. Numerical results are presented for each case.

Consider a region bounded by a rectangle with the length and width of a and b respectively, and containing a large central circular hole of radius ρ_0. Choose x and y axes parallel to the sides a and b of the rectangle with the origin at the center of the circular hole. Consider now the solutions of the nonhomogeneous equation

$$\nabla^2\phi_\ell=\delta(\rho-\rho_l)\cos 2\ell\varphi \tag{1a}$$

$$\nabla^2\equiv\frac{\partial^2}{\partial\xi^2}+\frac{\partial^2}{\partial\eta^2}\quad \rho_l<\rho_0\quad \ell=0,\ 1,\ 2,\ \ldots\quad \xi=\frac{x}{a}\quad \eta=\frac{y}{a} \tag{1b}$$

in which ρ and φ are the polar coordinates at the origin, and δ is the unit impulse function. Obviously, the solutions for ϕ_ℓ satisfy Laplace's equation for $\rho\geq\rho_0$. In addition, if these solutions satisfy the conditions

$$\phi_\ell=0 \quad \text{at} \quad \xi=\pm\tfrac{1}{2} \quad \text{and} \quad \eta=\pm\frac{b}{2a} \tag{2}$$

then they are the desired eigenfunctions mentioned earlier. To solve Eq. (1), subject to the conditions of Eq. (2), we first obtain Green's function. Let $\bar{\phi}$ be the solution of

$$\nabla^2\bar{\phi}=f(\xi,\eta,\xi_l,\eta_l) \quad \text{in rectangle} \quad a\times b \tag{3}$$

in which

$$f(\xi,u,\xi_l,\eta_l)=\dot{p}^*[\delta(\xi+\xi_l)+\delta(\xi-\xi_l)] \quad \text{for} \quad \eta_l>\eta>-\eta_l \tag{4a}$$

$$\xi_l,\eta_l<\rho_0 \quad \dot{p}=\text{const} \quad \text{(region I)} \tag{4b}$$

$$f(\xi,\eta,\xi_l,\eta_l)=0 \quad \text{for} \quad \eta>\eta_l \quad \text{and} \quad \eta<-\eta_l \quad \text{(region II)} \tag{4c}$$

Assuming an η independent particular integral of Eq. (3), the appropriate solution $\bar{\phi}_1$ for region I satisfying the homogeneous conditions at $\xi=\pm\frac{1}{2}$ can be written in the form

$$\bar{\phi}_1=\lambda_l(\xi)+\sum_{n=1,3,5\ldots}^{\infty}A_n\cosh n\pi\eta\cos n\pi\xi \quad \text{for} \quad \eta_l\geq\eta\geq-\eta_l \tag{5}$$

where

$$\lambda_l(\xi)=p^*(\xi-\tfrac{1}{2}) \quad \text{for} \quad \xi>\xi_l \tag{6a}$$

$$\lambda_i(\xi)=0 \quad \text{for} \quad -\xi_l<\xi<\xi_l \tag{6b}$$

$$\lambda_l(\xi)=-p^*(\xi+\tfrac{1}{2}) \quad \text{for} \quad \xi<-\xi_l \tag{6c}$$

For region II, we need consider only the solution for $\eta\geq\eta_l$ due to the symmetry. The solution $\bar{\phi}_{II}$ for this region automatically satisfying the homogeneous conditions at $\xi=\pm\frac{1}{2}$ and $\eta=b/2a$ can now be written as follows

$$\bar{\phi}_{II}=\sum_{n=1,3,5,\ldots}^{\infty}A_n^*\sinh n\pi\left(\eta-\frac{b}{2a}\right)\cos n\pi\xi \quad \text{for} \quad \eta\geq\eta_l \tag{7}$$

Here in Eqs. (5) and (7), A_n and A_n^* are the unknown constants of integration to be determined from the continuity conditions of the functions $\bar{\phi}$ and $\partial\bar{\phi}/\partial\eta$ at $\eta=\eta_l$. Expanding $\lambda_l(\xi)$, defined in Eqs. (6), in Fourier series and employing these continuity conditions, one obtains

$$A_n=-\frac{\beta_n\cosh n\pi(\eta_l-b/2a)}{\cosh(n\pi b/2a)} \tag{8a}$$

$$A_n^*=-\frac{\beta_n\sinh n\pi\eta_l}{\cosh(n\pi b/2a)} \tag{8b}$$

$$\beta_n=4p^*[-(1/n^2\pi^2)\cos n\pi\xi_l-(1/n\pi)\xi_l\sin n\pi\xi_l] \tag{8c}$$

Let us now consider a function $\bar{\phi}^0$ which satisfies

$$\nabla^2\bar{\phi}^0=f(\xi,\eta,\xi_l,\eta_l-\epsilon) \quad \text{in rectangle} \quad a\times b \tag{9}$$

Received April 7, 1975; revision received July 14, 1975. The computation portion of this project was supported by IUPUI Computing Services.

Index categories: Structural Static Analysis; Heat Conduction.

*Professor of Aeronautical-Astronautical Engineering and Mathematical Sciences.